Published in final edited form as:

J Phys Chem B. 2021 December 23; 125(50): 13696–13709. doi:10.1021/acs.jpcb.1c08245.

On the Role of the Conserved Histidine at the Chromophore Isomerization Site in Phytochromes

Anastasia Kraskov,
Institut für Chemie, Technische Universität Berlin, D-10623 Berlin, Germany

David Buhrke,
Institut für Chemie, Technische Universität Berlin, D-10623 Berlin, Germany; Present Address: Department of Chemistry, University of Zürich, Winterthurerstr. 190, CH-8057 Zürich, Switzerland

Patrick Scheerer,
Charité—Universitätsmedizin Berlin, Corporate Member of Freie Universität Berlin and Humboldt-Universität zu Berlin, Institute of Medical Physics and Biophysics, Group Protein X-ray Crystallography and Signal Transduction, D-10117 Berlin, Germany

Ida Shaef,
Institut für Chemie, Technische Universität Berlin, D-10623 Berlin, Germany; Present Address: Institut für Biotechnologie, Technische Universität Berlin, Sekr. TIB 4/3-2, Gustav-Meyer-Allee 25, D-13355 Berlin.

Juan C. Sanchez,
Department of Biology, Northeastern Illinois University, Chicago, Illinois 60625, United States

Melissa Carrillo,
Department of Biology, Northeastern Illinois University, Chicago, Illinois 60625, United States

Moraima Noda,
Department of Biology, Northeastern Illinois University, Chicago, Illinois 60625, United States

Denisse Feliz,
Department of Biology, Northeastern Illinois University, Chicago, Illinois 60625, United States

Emina A. Stojković,
Department of Biology, Northeastern Illinois University, Chicago, Illinois 60625, United States

Peter Hildebrandt
Institut für Chemie, Technische Universität Berlin, D-10623 Berlin, Germany

Corresponding Authors: Patrick Scheerer – Charité—Universitätsmedizin Berlin, Corporate Member of Freie Universität Berlin and Humboldt-Universität zu Berlin, Institute of Medical Physics and Biophysics, Group Protein X-ray Crystallography and Signal Transduction, D-10117 Berlin, Germany; patrick.scheerer@charite.de, **Peter Hildebrandt** – Institut für Chemie, Technische Universität Berlin, D-10623 Berlin, Germany; peter.hildebrandt@tu-berlin.de.

Supporting Information

The Supporting Information is available free of charge at https://pubs.acs.org/doi/10.1021/acs.jpcb.1c08245.
Further UV–vis absorption and RR spectra of the five phytochrome variants (PDF)

Complete contact information is available at: https://pubs.acs.org/10.1021/acs.jpcb.1c08245

The authors declare no competing financial interest.

Abstract

Phytochromes are sensory photoreceptors that use light to drive protein structural changes, which in turn trigger physiological reaction cascades. The process starts with a double-bond photoisomerization of the linear methine-bridged tetrapyrrole chromophore in the photosensory core module. The molecular mechanism of the photoconversion depends on the structural and electrostatic properties of the chromophore environment, which are highly conserved in related phytochromes. However, the specific role of individual amino acids is yet not clear. A histidine in the vicinity of the isomerization site is highly conserved and almost invariant among all phytochromes. The present study aimed at analyzing its role by taking advantage of a myxobacterial phytochrome SaBphP1 from *Stigmatella aurantiaca*, where this histidine is naturally substituted with a threonine (Thr289), and comparing it to its normal, His-containing counterpart from the same organism SaBphP2 (His275). We have carried out a detailed resonance Raman and IR spectroscopic investigation of the wild-type proteins and their respective His- or Thr-substituted variants (SaBphP1-T289H and SaBphP2-H275T) using the well-characterized prototypical phytochrome Agp1 from *Agrobacterium fabrum* as a reference. The overall mechanism of the photoconversion is insensitive toward the His substitution. However, the chromophore geometry at the isomerization site appears to be affected, with a slightly stronger twist of ring D in the presence of Thr, which is sufficient to cause different light absorption properties in SaBphP1 and SaBphP2. Furthermore, the presence of His allows for multiple hydrogen-bonding interactions with the ring D carbonyl which may be the origin for the geometric differences of the C–D methine bridge compared to the Thr-containing variants. Other structural and mechanistic differences are independent of the presence of His. The most striking finding is the protonation of the ring C propionate in the Pfr states of SaBphP2, which is common among bathy phytochromes but so far has not been reported in prototypical phytochromes.

Graphical Abstract

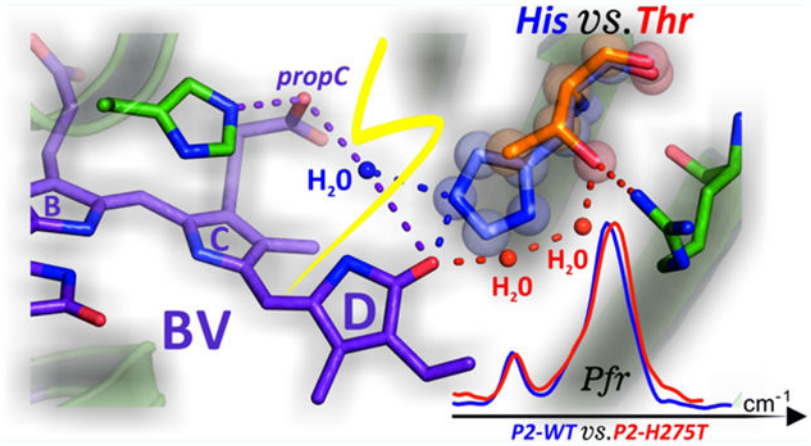

INTRODUCTION

Many light-dependent physiological processes are controlled by phytochromes which photoconvert between the inactive and active states, denoted as Pr and Pfr according to their absorption in red and far-red spectral regions, respectively.[1–4] These photoreceptors,

found in plants, bacteria, and fungi, are composed of several modules. They include the N-terminal photosensory core module (PCM), carrying a covalently bound, open-chain tetrapyrrole cofactor. PCM is typically composed of a PAS (Per/Arndt/Sim-), GAF (cGMP phosphodiesterase/adenyl cyclase/FhlA-), and PHY (phytochrome-specific-) domain.[2,3,5] It is linked to a C-terminal output module, usually an enzymatic domain such as a histidine kinase. Although phytochromes of different origins display a considerable variability, for instance, in terms of module composition, type of the bilin chromophore, and its attachment site in the protein, the light-induced reaction cascade of PCM follows very similar mechanistic patterns in all representatives of this important photoreceptor family.[2,6] Upon light absorption in the Pr state, the tetrapyrrole undergoes an isomerization at the methine bridge between rings C and D from the *ZZZssa* configuration to the *ZZEssa* configuration (Figure 1).[2,7] The resulting strained chromophore geometry in the primary photoproduct (Lumi-R)[8] then thermally relaxes to the Meta-Ra state, presumably accompanied by minor positional and orientational adjustments of the surrounding amino acids.[6,9] The subsequent processes that eventually lead to the Pfr state include proton-transfer steps[10,11] and a secondary structure transition of the tongue segment in the PHY domain.[12] The latter is a key event since it induces further tertiary and quaternary structural changes that expand beyond PCM and ultimately regulate the output domain and enable its function.[13,14] A similar albeit not identical mechanistic pattern holds for the Pfr → Pr photoconversion.[2,7] However, despite intensive efforts, a comprehensive understanding of parameters that control the molecular mechanism of Pr/Pfr phototransformation and, in particular, the coupling of chromophore and protein structural changes is still lacking.

One important question refers to the role of the highly conserved amino acids in the chromophore binding pocket. This issue has been addressed in the past by site-directed mutagenesis of various phytochromes and analyzing the impact on the structure and reaction mechanism by X-ray crystallography and spectroscopy.[15–17] It was found, for example, that Asp in the conserved *PASDIP* motif serves as a bridge between the pyrrole N–H groups and the *PRXSF* motif in the sensory tongue and helps stabilizing the secondary structure of the tongue. It is thus indispensable for the photoconversion of the Pr state in all phytochromes.[18,19] However, for other conserved amino acids such as the highly conserved His located directly near the isomerization site and the propionic side chain of ring C (propC), substitution experiments on different bacteriophytochromes did not yield consistent results.[15,20] This His forms a hydrogen bond to the ring D carbonyl group in the Pr state. It thus stabilizes the *ZZZssa* conformation of the chromophore, whereas in the Pfr state, it is involved in coordination of prop*C*, as indicated by crystal structures of prototypical and bathy phytochromes.[17,21–25] In the prototypical phytochrome from *Deinococcus radiodurans*, *Dr*BphP, the replacement of the conserved His290 with Gln blocks the Pr → Pfr photoconversion at the Meta-Rc state,[15] and replacement with Thr reduces the extent of Pfr formation.[26] In the bathy phytochrome from *Pseudomonas aeruginosa*, *Pa*BphP, in which Pfr is the dark-adapted state, replacement of His277 with Ala converts the photoreceptor into a prototypical phytochrome with Pr as the stable dark state.[20] In contrast, substitution of His278 with Ala or Gln in the homologous bathy phytochrome of *Agrobacterium fabrum*, Agp2, solely slows down the dark reversion from Pr to Pfr.[27,28]

In this respect, the two phytochromes, SaBphP1 and SaBphP2, from *Stigmatella aurantiaca* offer a promising alternative to analyze the role of this conserved histidine in the Pr → Pfr photoconversion.[29,30] Here, the corresponding His (His275) is only conserved in SaBphP2 but replaced with a Thr (Thr289) in SaBphP1 (Figure 2). Beside this difference, the amino acid composition in the chromophore binding pocket is largely identical between these two BphPs, the first myxobacterial BphPs that were characterized (Figure 2).

The physiological significance of the His substitution observed primarily in myxobacterial phytochromes is not yet understood. It is important to note that the His-lacking variants were only found in those myxobacteria species that contain at least one more BphP where the conserved histidine is present.[29] The PCMs of both proteins share the typical PAS-GAF-PHY architecture with the sensory tongue organized in a β-sheet and the biliverdin (BV) chromophore in the *ZZZssa* configuration as a characteristic of the Pr state of all BphPs.[29,30] Although molecular details of their function are yet unknown, X-ray scattering data suggest that the signal transduction in the full-length SaBphP1 and SaBphP2 is associated with similar conformational changes upon the photoconversion as in other phytochromes.[31] Moreover, crystal structures are available for the Pr states of SaBphP1 and SaBphP2 and their respective single amino acid mutants, SaBphP1-T289H and SaBphP2-H275T.[29,30] Most recently, room-temperature crystal structures of 5 ns and 33 ms intermediates after light illumination of the Pr state of wild-type (WT) SaBphP2 have been determined, providing important insight into structural displacements of the BV chromophore and neighboring amino acids.[32] Additionally, the WT SaBphP1 has already been characterized by transient UV–vis and IR spectroscopy.[26]

In this work, we have studied the Pr → Pfr photoconversion of four phytochrome variants from *S. aurantiaca* by resonance Raman (RR) and IR difference spectroscopy. Two variants contained the conserved His (SaBphP2 and SaBphP1-T289H) which in the other two was replaced with a Thr (SaBphP1 and SaBphP2-H275T). We used the structurally and spectroscopically well-characterized prototypical bacteriophytochrome Agp1 from *A. fabrum* as a reference model[11,16,25,33–38] to identify structural differences between these phytochrome variants related to the conserved histidine and its role in the Pr → Pfr photoconversion.

EXPERIMENTAL SECTION

Protein Expression and Assembly.

All phytochromes were expressed and purified as PCMs. Myxobacterial SaBphP1 and SaBphP2 WT and mutant variants were expressed and purified as described previously.[29,30] Agp1 was expressed and purified as described previously.[16,39] For vibrational spectroscopic experiments, the buffered solution of the purified protein was concentrated up to an optical density at 750 nm of ca. 40 using an Amicon centrifugal filter (MWCO 30 K, 15 800*g*, 4 °C). H/D exchange was achieved by the same procedure but using a buffered solution in D_2O (pD 7.8). For the IR absorption measurements, the sample was incubated overnight in D_2O buffer, followed by another concentration/dilution cycle.

RR Spectroscopy.

RR measurements were performed using a Bruker Fourier-transform Raman spectrometer RFS 100/S with 1064 nm excitation (Nd-YAG cw laser, line width 1 cm^{-1}), equipped with a nitrogen-cooled cryostat from Resultec (Linkam).[28] All spectra of the samples in the frozen solution were recorded at ca. 90 K with a laser power at the sample of 690 mW and an accumulation time of typical 1 h. In order to identify potential laser-induced damage of the phytochrome samples, RR spectra before and after a series of measurements were compared. In no case, changes between these control spectra were determined. Protein and buffer Raman bands were subtracted on the basis of a Raman spectrum of apo-phytochrome. To probe the Pfr state, the sample was illuminated for 1 min using a light-emitting diode (LED) (λ = 660 nm) at ambient temperature, whereas for intermediates of the Pr → Pfr photoconversion, an irradiation temperature was chosen that was sufficiently low to block the decay of the desired intermediate. After photoconversion, the sample was cooled to 90 K for the Raman measurement. Residual contributions from the unphotolyzed state or unwanted decay products were removed by spectra subtraction using the OPUS software (Bruker). A more detailed description is given elsewhere.[40]

IR and UV–Vis Spectroscopy.

IR spectroscopic measurements were carried out in the transmission mode at 20 °C using a Bruker Tensor 27 or IFS66v/s Fourier transform infrared spectrometer.[28] Spectra were recorded with 200 single scans and a spectral resolution of 2 cm^{-1} and the double-sided acquisition mode. The Pr-to-Pfr conversion was achieved by continuous sample illumination with built-in diode arrays (780 and 670 nm). Difference spectra were recorded by subtraction of the initial state spectrum from the illuminated state spectrum. The UV–vis measurements were performed using a Varian Cary 50 Bio UV–vis spectrophotometer (Agilent). The protein sample was diluted (OD at 750 nm of ca. 0.25) and illuminated with a 644 nm LED for photoconversion.

Sequence Alignment.

The alignment in Figure 2G was visualized using the software BioEdit.[41] Background colors indicating conservation (Blossum62 matrix) among different receptors and reflecting chemical properties of the amino acid side chains: black—proline, blue—positively charged, cyan/green—aromatic and hydrophobic, green—hydrophobic, red—negatively charged, gray—hydrophilic, dark red—cysteines, and magenta—histidine.

RESULTS

We have recorded the RR spectra of the four SaBphP1 and SaBphP2 WT and mutant variants in the parent and the intermediate states of the Pr-to-Pfr (Pr → Pfr) photoconversion. These spectra as well as the respective “Pfr minus Pr” IR difference spectra were compared to those of Agp1 in view of its comprehensive structural and spectroscopic characterization.[11,16,25,33–38] In particular, vibrational assignments for the various states of Agp1, inter alia based on isotopic labeling and computational methods,[38,40] can readily be adopted to analyze the spectra of the various SaBphP1 and SaBphP2 states. We will focus on those modes for which correlations with structural parameters are

established.[38,42,43] These modes are largely localized in specific parts of the chromophore, as illustrated in Figure 1.

None of the *S. aurantiaca* phytochromes studied here exhibited a full photoconversion characterized by a distinct shift of the Q-band absorption. Instead, an absorption increase around 760 nm is observed upon illumination with 644 nm light. This change is more pronounced in SaBphP2-WT and SaBphP1-T289H, indicating a larger extent of Pr → Pfr photoconversion in the His-containing variants compared to those lacking the conserved His, that is, the Thr-containing variants SaBphP1-WT and SaBphP2-H275T (Figure S1). Thus, the individual parent states could be largely enriched by appropriate irradiation, but none of them was obtained in a pure form. This is attributed to the spectral overlap which does not allow for exclusive excitation of either Pr or Pfr. This also has a consequence for the RR spectroscopic analysis. Generation of the pure RR spectra of Pr and Pfr as well as the intermediates of the Pr → Pfr photoconversion required subtraction procedures as described in detail elsewhere.[40] Hence, all RR spectra shown in this work represent pure states.

RR Spectra of the Parent States.

In each parent state, that is, Pr and Pfr, the RR spectra of all four SaBphP variants display a very similar vibrational signature that is closely related to that of other prototypical bacteriophytochromes such as Agp1 (Figures 3 and 4).[11,15,16,35,40,42,44] These similarities include the structural heterogeneity that is evidenced by the pairwise appearance of specific localized modes, such as the C=C stretching of the A–B methine bridge (A–B stretching; 1639–1652 cm^{-1}) in the Pr state (Figure 3)[35,40,44] and the hydrogen out-of-plane mode of the C–D methine bridge (HOOP; 804–818 cm^{-1}) in the Pfr state (Figure 4).[42] For Agp1, the relative intensities of the two HOOP components were shown to vary with the temperature, demonstrating a temperature-dependent equilibrium between two conformational sub-states.[42] In view of the similarities in the A–B stretching (Pr) and HOOP regions (Pfr), we, therefore, conclude that such conformational equilibria also exist in the parent states of the four SaBphP variants.

The strongest signal in the RR spectrum originates from the C–D methine bridge stretching at ca. 1625 and 1600 cm^{-1} in Pr and Pfr, respectively (Figures 3 and 4).[38,42] It is accompanied by a closeby stretching mode of ring D. Both the HOOP and C–D stretching frequencies are correlated with geometrical parameters of the C–D methine bridge.[38,42,43] In the Pr state of the SaBphP variants, the frequencies of the C–D stretching mode are downshifted by 2–5 cm^{-1} compared to Agp1, corresponding to a smaller deviation of the single-bond dihedral angle from the ideal planar anti-conformation (Figure 3). The dihedral angle of the double bond also appears to be closer to 0° as suggested by the upshift of the HOOP mode frequency which is inversely correlated with the double-bond torsion. Taking into account that the rotations described by these correlations are associated with opposite signs and thus may partially compensate, the overall twist angle between both rings equals the sum of both dihedral angles, which in turn should be proportional to the difference between the C–D stretching and HOOP mode frequencies. Accordingly, one would expect a higher torsion of the C–D methine bridge for the His-lacking SaBphP1-WT and SaBphP2-H275T compared to the His-containing SaBphP2-WT. In view of the crystal structures,[29,45]

also, SaBphP1-T289H is expected to fit into this scheme, although the analysis of the RR spectrum is impaired due to the heterogeneity of the HOOP mode (Figure 3).

In the Pfr state, the frequencies of the C–D stretching modes are 1–4 cm^{-1} upshifted compared to Agp1 (Figure 4), pointing to an increased deviation of the single-bond dihedral angle from the ideal anti-conformation. The HOOP frequencies, instead, remain largely unchanged compared to Agp1 except for a slight decrease in SaBphP2-H275T. Thus, the C–D methine bridge of the SaBphP variants in the Pfr state exhibits a slightly larger torsion than Agp1. This is more pronounced in the Thr-containing variants, especially if compared to their respective His-containing counterparts. Note that the sensitivity of these frequency–structure correlations is in the order of 1 cm^{-1}/degree,[43] and thus, these changes in the geometry are likely beyond the level of detection of the standard protein X-ray crystallography under cryogenic conditions.

Further differences, particularly in the Pr state, refer to the region between 640 and 680 cm^{-1} that is dominated by modes with large contributions of torsional (tors) and out-of-plane (oop) coordinates of ring D and the C–D methine bridge (Figures 3 and 4). The changes mainly refer to variations of the relative intensities, whereas the band positions remain largely unchanged. This is also true for the region between 1280 and 1330 cm^{-1}. These bands originate from modes with contributions from the N–H in-plane bending (NH ip) coordinates of rings A and D, as supported by the drastic alterations upon H/D exchange (Figure 5). The corresponding NH ip coordinates of rings B and C are largely localized in two modes. One of them is RR-active and gives rise to a band at ca. 1570 and 1550 cm^{-1} in Pr and Pfr, respectively (Figures 3 and 4). The frequency of this mode does not vary significantly, indicating similar hydrogen-bonding interactions associated with the pyrrole nitrogens in all proteins under study, regardless of the presence of the conserved His.

Intermediates of the Photoinduced Pr → Pfr Conversion.

In prototypical phytochromes, the photoconversion from Pr to Pfr runs via a sequence of three intermediates (Figure 1), which were also identified in the four SaBphP variants by cryogenic trapping.[40] Each of these intermediates displays a characteristic pattern of vibrational bands, particularly in the “marker band region” between 1500 and 1700 cm^{-1} (Figures 5 and S2–S5).

In Agp1, the first intermediate Lumi-R could be trapped between 130 and 190 K, with an optimum at ca. 170 K.[40] For the SaBphP variants, trapping was successful only at higher temperatures (170—190 K). In Lumi-R, the chromophore adopts a distorted *ZZEssa* geometry with a substantial twist of the C–D methine bridge as reflected by the frequency shifts of the modes localized in this part of the chromophore. In Pr, the prominent RR band at ca. 1625 cm^{-1} is composed of two closely spaced modes, that is, the C–D double-bond stretching and the C=C stretching in ring D.[38] Both modes are clearly separated in SaBphP1-WT, SaBphP1-T289H, and SaBphP2-WT and in Agp1 alike since the ring D C=C stretching undergoes only a moderate downshift by 5–10 cm^{-1} compared to the Pr state. In Lumi-R, it is found at ca. 1620 cm^{-1}, whereas the downshift of the C–D stretching is about 30 cm^{-1} toward ca. 1595 cm^{-1} (Figures 5, 6, S5, and S6).[40] In contrast, SaBphP2-H275T shows a downshift of the C–D stretching frequency by only ca. 20 cm^{-1}, while the ring

D C=C stretching cannot be identified. The HOOP mode displays an upshift compared to Pr by 11–14 cm^{-1} in all variants except the His-lacking SaBphP1-WT, where a distinctly larger upshift of 25 cm^{-1} is observed. Due to the different mode composition in the distorted *ZZEssa* configuration of Lumi-R,[40] it is not justified to adopt the correlations between frequencies and dihedral angles as established for the chromophore configurations of the parent states also to Lumi-R (*vide supra*). However, one may take the deviating behavior in the Thr-containing SaBphP1-WT (HOOP) and SaBphP2-H275T (C–D stretching) variants as an indication for different twists of ring D with respect to ring C compared to the His-containing SaBphP variants as well as Agp1. The A–B stretching modes in Lumi-R are more difficult to identify due to their relatively low intensity. As exemplarily shown for SaBphP2-WT, H/D exchange reveals two bands attributable to the A–B stretching of the two conformational substates (Figure 5). In contrast to Agp1, where the A–B stretching modes of both conformers display the same ca. 10 cm^{-1} downshift upon the Pr → Lumi-R transition (Figure 6),[40] this appears to hold only for the lower-frequency component of SaBphP2-WT, whereas the higher-frequency component remains largely unchanged. This behavior is common to all SaBphP variants as far as the modes can be identified with confidence (Figure 6). Particularly remarkable in all Lumi-R spectra are the intense bands in the N–H/C–H ip region which is dominated by a peak at ca. 1312 cm^{-1} (Figure S6). These bands largely disappear upon H/D exchange (Figure 5), indicating the contribution of the N–H ip coordinates of rings A and D to these modes.[27,42]

In the Meta-Ra state which is trapped between 210 and 250 K, the C–D methine bridge and ring D C=C stretching modes display opposite frequency shifts compared to Lumi-R such that they move toward each other (Figures 7 and S7). Due to the close energetic and spatial proximity of both modes, the underlying coordinates most likely mix as indicated by the similar H/D isotopic shifts originating from the N–H ip coordinates of rings C and D (Figure 5). Meta-Ra includes a largely relaxed *ZZEssa* chromophore structure, and the frequencies of the C–D and ring D stretching modes shift toward those of the final Pfr state. In all four SaBphP variants, the corresponding bands now can be found between 1595 and 1612 cm^{-1}. In SaBphP2-H275T, the chromophore geometry appears to be particularly close to that of the Pfr state, in view of the almost identical C=C stretching band positions in Meta-Ra and Pfr. In contrast to this, Agp1 shows one band at a distinctly higher frequency (1621 cm^{-1}). Most remarkable, however, is the band pattern of the His-containing SaBphP1-T289H and SaBphP2-WT. It includes two separated bands at 1610–1612 and 1595–1599 cm^{-1}, pointing to a specific geometry of the C–D methine bridge in these two variants as opposed to their Thr-containing counterparts. We attribute these bands to two modes, each of them involving both the C–D and ring D stretching coordinates in view of the same H/D shifts. An alternative interpretation is based on a conformational equilibrium between two sub-states, characterized by distinctly different C–D stretching modes. In this case, the spectral differences between SaBphP1-T289H/SaBphP2-WT and SaBphP2-H275T/SaBphP1-WT might reflect different relative populations of the two sub-states, with the higher-frequency mode being more dominant in the His-containing variants.

In all four SaBphP variants, only one A–B stretching mode can be identified at 1631 cm^{-1}, which is at a distinctly lower frequency than in Agp1 (Figure 7). Disappearance of the A–B stretching doublet which persisted during Pr and Lumi-R suggests that the structural

differences between both conformers of the A–B methine bridge are largely removed in the Meta-Ra state.

Upon the decay to Meta-Rc, which is trapped between 240 and 260 K, a proton is released from either the ring B or ring C N–H group, followed by a proton re-uptake in the last step, the formation of Pfr.[11,16,37,40] Thus, Meta-Rc is the only intermediate with a deprotonated tetrapyrrole chromophore as readily detected by the lack of the NH ip bending of rings B and C between 1550 and 1580 cm^{-1} (Figures 5, 7, and S8). As a consequence, the composition of the normal modes that are localized in rings C and B is now quite different from that in protonated tetrapyrroles.[9,46–48] The C=C stretching region is dominated by two broad and overlapping bands at 1580–1590 and 1600–1610 cm^{-1}. While the frequencies differ somewhat between Agp1 and the four SaBphP variants, there appears to be an intensity pattern. However, in Agp1 and SaBphP1-T289H, the lower-frequency component at ca. 1590 cm^{-1} dominates over a higher-frequency band, and the intensity ratio is reversed in SaBphP1-WT, SaBphP2-WT, and SaBphP2-H275T. This does not appear to correlate with the presence or absence of the conserved histidine. Interestingly, a high intensity of the 1590 cm^{-1} band is accompanied by a distinct intensity increase of two bands at 973 and 1094 cm^{-1} (Figure S8), with the latter in the range expected for C–N stretching coordinates.[46] The different intensity ratios in the C=C stretching region most likely reflect the distribution between BV species which are protonated at either ring B (B-protonated) or ring C (C-protonated).

Protein Structural Changes during the Pr → Pfr Transition.

The “Pfr minus Pr” IR difference spectra primarily reflect the protein structural changes during the Pr → Pfr transition, that is, the refolding of the sensory tongue segment (Figure 8).[12,27,28,49] In fact, all SaBphP variants show the expected positive bands between 1654 and 1658 cm^{-1} and negative bands between 1631 and 1636 cm^{-1} that reflect the formation of an α-helix (Pfr) at the expense of the β-sheet/hairpin structure. In contrast to these amide I bands, the amide II difference signals around 1550 cm^{-1} are very weak in each case. In addition to the protein bands, the IR difference spectra also include signals from IR-active tetrapyrrole modes, which are the C=C stretching of the B–C methine bridge (B–C stretching; ca. 1580 and 1590 cm^{-1} in Pfr and Pr, respectively)[37,50,51] and the particularly indicative C=O stretching modes of rings A and D, expected in the frequency range between 1680 and 1740 cm^{-1}.

C=O Stretching Modes of Rings D and A.

In the SaBphP variants, this region displays a vibrational pattern that differs substantially from that of Agp1[37] such that the identification of the individual C=O modes is not straightforward. We have thus included the RR spectra to obtain additional assignment criteria. Although the RR activity of these modes is rather low with less than 4% of the peak intensity of the C–D stretching and they can only be detected in the parent states, RR spectroscopy offers the advantage of measuring absolute bands and thus avoids the superposition of positive and negative signals, as illustrated in Figure 9. The assignment of the bands takes into account that the C=O stretching of ring A appears at higher frequencies than that of ring D, in line with theoretical calculations.[28,37,38] In most cases, there is good

agreement of the RR peaks with the IR difference signals. Deviations are attributed to partial compensation of negative and positive signals in the IR difference spectra such that the frequencies were primarily determined from the RR spectra. However, in those cases where the signal-to-noise ratio of the RR spectrum impaired a safe determination of the peak position, we relied on the difference peaks in the IR spectra. Further support for the assignments was derived from the H/D isotopic shifts, which are in general between 5 and 10 cm^{-1}.

In the Pfr state, the RR spectra of all five proteins display a prominent band between 1710 and 1713 cm^{-1}, which hence is attributed to the C=O stretching of ring D. Only for the SaBphP2-H275T variant, this band hardly exceeds the noise level, but it is clearly detectable in the IR difference spectrum. In addition, all proteins show a positive IR signal between 1682 and 1686 cm^{-1} which is located in a spectral region of either the chromophore C=O stretching or the amide I modes.[12,26,52,53] However, these signals can be related to bands in the RR spectra, thus arguing in favor of a BV mode. Furthermore, time-resolved IR data revealed a rise time of this band on the picosecond time scale,[26] which is too short for secondary structure changes. Thus, we assign these bands to the C=O stretching of a minor conformational sub-state of Pfr in addition to the major fraction reflected by the band between 1710 and 1713 cm^{-1}. In fact, this conformational heterogeneity is not surprising since it parallels the splitting of the HOOP mode of the C–D methine bridge (*vide supra*).

The corresponding C=O stretching of ring A appears between 1718 and 1726 cm^{-1} with distinctly weaker intensity in the IR and RR spectra, consistent with theoretical predictions.[38] The only exception refers to SaBphP1-WT with relatively intense IR and RR signals and an additional RR band component at 1734 cm^{-1}, which displays a downshift of 7 cm^{-1} upon H/D exchange, typical of C=O stretching modes in tetrapyrroles. We therefore attribute this band to a second C=O stretching of ring A, reflecting a structural heterogeneity at ring A.

Following the same rationale, we now turn to the assignment of the C=O stretching modes in Pr. Here, the intensities of the RR bands and the negative IR signals are distinctly weaker compared to Pfr such that in some cases, identification of the modes was associated with some ambiguities. The structural heterogeneity at the C–D and A–B methine bridges is not in each case reflected by two C=O stretching modes of the respective rings. In Agp1, only a single C=O stretching of ring A is observed, while SaBphP1-WT and SaBphP2-WT show just one ring D C=O stretching mode. In all the other cases, the corresponding modes appear pairwise, as listed in Figure 9. For the SaBphP2-H275T variant, the assignments may be debatable since—as for Pfr—the poor S/N ratio of the RR spectra prohibits the detection of these bands.

The present assignments of the C=O modes require two additional comments. First, the two bands at 1711 and 1686 cm^{-1} in the Pfr state of SaBphP2-WT, attributed to the C=O stretching of ring D, are essentially insensitive to H/D exchange, in contrast to the typically observed H/D shifts between 5 and 13 cm^{-1} (Figure 9). These shifts result from coupling of the N–H bending with the C=O stretching coordinate. This coupling, however, can be reduced if, for instance, the N–H bond is tilted out of the ring D plane. Such a tilt could be

induced by specific hydrogen-bonding interactions in the Pfr state of SaBphP2-WT. Second, in the Pr state of both SaBphP1 variants, the RR intensity of the ring D C=O stretching modes is distinctly weaker than their ring A counterparts. We have currently no plausible explanation for this unexpected observation that contradicts theoretical calculations.[38]

C=O Stretching of the Ring C Propionic Side Chain.

A particularly remarkable finding refers to the SaBphP2 variants. The IR difference spectra display a distinct positive peak at 1748 cm^{-1}, which shifts down by 7 cm^{-1} in D_2O (Figure 9). Additionally, SaBphP2-H275T displays a somewhat weaker negative signal at 1759 cm^{-1} (1751 cm^{-1} in D_2O), which is, however, missing in SaBphP2-WT. These observations resemble the situation in bathy phytochromes, where the propionic side chain of ring C (propC) is protonated in Pfr, as reflected by a band at essentially the same frequency.[27,54] We thus conclude that in SaBphP2-WT, propC is protonated in the Pfr state, whereas in the His-lacking SaBphP2-H275T, this BV side chain is partially protonated in Pr as well.

DISCUSSION

All SaBphP variants studied here reveal characteristic structural and mechanistic properties of prototypical phytochromes. The Pr → Pfr phototransformation runs via the same intermediates as the well-characterized phytochrome Agp1, including largely similar underlying chromophore and protein structural changes. Furthermore, we noted a chromophore structural heterogeneity as in Agp1, with two substates differing in subtle details of the A–B and C–D methine bridge conformations. Most likely, the four SaBphP variants undergo phototransformation via two parallel pathways as discussed previously for other prototypical phytochromes.[40] Perturbations of the ring D structure appear to play a special role in SaBphPs. In SaBphP1-WT, the excited state is heterogeneous, possibly giving rise to a portion of Lumi-R species where ring D flips back to the *ZZZssa* conformation.[45] A recent crystallographic study revealed a dual ring D conformation in a late intermediate state of SaBphP2-WT.[32] Interestingly, only in the SaBphP variants, regardless of the presence of the conserved His, the structural heterogeneity at the A–B methine bridge in the Pr state is accompanied by a splitting of the C=O stretching modes of ring A, whereas in Agp1, only a single band is observed (Figure 9). This difference may be related to the exocyclic attachment of ring A to the protein in SaBphP2 and, at least partially, SaBphP1. Although the published crystal structure of SaBphP1 shows ring A with endocyclic attachment (Figure 2), revisiting the structural data points to a mixed attachment mode with at least a fraction of exocyclic ring A attachment. Thus, due to the lack of an intra-ring double bond in SaBphP, ring A may increase the flexibility of the C=O group and its interactions with the immediate environment, in contrast to Agp1 with its endocyclic chromophore binding (see Figure 2).[25] It should be noted, however, that the conformational differences between the two sub-states may be so small that they are beyond the detection limit of crystallographic structure analysis.

In addition to the general similarities, there are some minor but notable differences in the structures of the chromophores and their interactions with the protein environment, some of

which are related to the presence or substitution of His at position 289 (SaBphP1) or 275 (SaBphP2).

Structural Differences Due to Specific Interactions of Ring D.

Most of the structural differences of the chromophore that may be related to the presence of the conserved His are localized at the isomerization site and thus in immediate vicinity to this amino acid. Hence, these differences evidently result from the direct interaction with ring D and the C–D methine bridge.

In Pr, frequencies of the HOOP and C–D stretching modes indicate a stronger twist of ring D in the variants that possess a Thr at the position of the conserved His. This is in agreement with the eight (here considered) PCM crystal structures [name-variant/PDB entry/resolution/experimental cryogenic/room temperature (CT/RT)]: SaBphP1-WT/6BAO/2.18 Å/CT,[29] SaBphP1-T289H/6BAP/2.65 Å/CT,[29] SaBphP1-T289H/6BAY/3.15 Å/RT,[29] SaBphP2-WT/6PTX/1.65 Å/CT,[30] SaBphP2-WT/6PTQ/2.1 Å/RT,[30] SaBphP2-H275T/6PU2/2.2 Å/CT,[30] Agp1-WT/5I5L/2.7 Å/CT,[25] Agp1-WT-(surface-mutant)/5HSQ/1.85 Å/CT,[25] of the three phytochromes SaBphP1, SaBphP2, and Agp1 (partially shown as chromophore pockets in Figure 2A–F). The structural data for SaBphP1 show that ring D is slightly rotated toward His289 in SaBphP1-T289H, thus affording a smaller twist of the C–D methine bridge compared to the threonine-containing SaBphP1-WT, in line with the RR spectroscopic data. The altered ring D orientation is accompanied by differences in ring D coordination. SaBphP2-H275T is largely devoid of hydrogen bonds toward the ring D C=O group (Figure 2F), whereas Thr-containing SaBphP1-WT (molecule B of the crystal structure) has direct hydrogen-bonding interactions with a water molecule (Figure 2C). In the His-containing SaBphP2-WT, SaBphP1-T289H, and Agp1, there is a hydrogen bond between the ring D C=O group and the conserved histidine. Additionally, the ring D C=O is hydrogen-bonded by a water molecule in SaBphP2-WT. In SaBphP1-T289H, Ser287 serves as a hydrogen-bond donor, which is unique for SaBphP1, since Agp1 and SaBphP2 have an alanine at the same position. The principal hydrogen-bond donor, the conserved His, is also stabilized by an arginine in Agp1 (Arg162), SaBphP2-WT (Arg157), and SaBphP1-T289H (Arg173) (Figure 2). In SaBphP2-WT, His275 is additionally coordinated by a water molecule, and in Agp1, interactions of the corresponding residue His280 involve a network of four water molecules. Together, these observations indicate a more rigid and well-ordered ring D environment in Agp1 and SaBphP2, as opposed to SaBphP1, and multiple interactions of the ring D C=O group in the His-containing variants. In fact, these interactions of the His-containing variants, Agp1, SaBphP1-T289H, and SaBphP2-WT are also reflected by the C=O (D) stretching modes for which at least one component is observed at distinctly higher frequencies (ca. 1715 cm^{-1}) than in the Thr-containing variants (≤1700 cm^{-1}) (Figure 9). In SaBphP2-H275T, the distance between the ring D C=O group and a water molecule near propC is very weak or slightly too long (3.6 Å) for strong hydrogen-bonding interactions (Figure 2F). Of note, the 1.4 Å-resolution H290T mutant crystal structure of PAS-GAF from the *D. radiodurans* phytochrome shows additional water molecules between ring D and Thr, filling the gap created by this mutation.[26] IR data suggest that the ring D C=O group is more strongly coordinated by hydrogen bonds when the histidine is absent.[26] In the case of SaBphP2-H275T, such additional water molecules are probably also present but have

not been detected in the electron density because of the possible high flexibility. However, in contrast to the Thr-containing *D. radiodurans* variant, in SaBphP2-H275T, both Arg157 (Figure 2F) and Met252 (not shown) are slightly rotated into this gap, reducing the free space for further interacting water molecules. In case of the Thr-containing SaBphP1-WT (only for molecule B of the crystal structure), a hydrogen-bonded water molecule is visible in this gap.

An interesting difference to Agp1 (with Ser264) is that in all SaBphP1 and SaBphP2 variants, Ser271/Ser257 forms a direct connection to the propC-water-ring D hydrogen-bonding network (Figure 2).

A less distorted C–D methine bridge is associated with a higher extent of π-electron conjugation and may be a plausible explanation for the red shift of the Pr UV–vis absorption maxima in the His-containing variants (707, 703, and 703 nm in SaBphP1-T289H, SaBphP2-WT, and Agp1, respectively) compared to the Thr-containing SaBphP1-WT and SaBphP2-H275T (702 nm in both cases) (Figure S1). Possibly, also, the well-ordered and more rigid BV environment as observed in the Pr state of His-containing variants (*vide supra*) may contribute.[29] For the Pfr state, our Raman data also suggest a larger twist of the C–D methine bridge in the Thr-containing variants. This may explain the blue shift of the Pfr absorption maxima in these variants and the apparently lower yield of Pfr formation.[26]

The slightly different geometry of the C–D methine bridge in the presence of an adjacent Thr or His also affects the structures of the intermediates. In Lumi-R, ring D likely adopts a different twist angle with respect to ring C in SaBphP1-WT and SaBphP2-H275T compared to the other variants that include the conserved His. Accordingly, the present data are consistent with the previous suggestion that the substitution of His275/289 by Thr alters the primary photochemical process, possibly via a higher flexibility and/or additional water molecules around the ring D environment.[26] The effect of His → Thr substitution is also clearly visible in the subsequent Meta-Ra intermediate on the basis of the stretching modes localized at the C–D methine bridge and ring D due to either a specific structural change or a shift of the conformational equilibrium (Figure 7).

Structural Differences between SaBphP1 and SaBphP2.

Not all structural differences between the various phytochrome variants are associated with the presence or absence of the conserved His. Instead, some of them distinguish between the SaBphP1 and SaBphP2 variants, regardless of the conserved His. The most striking finding refers to propC, which is protonated in the Pfr state of both SaBphP2 proteins but deprotonated in SaBphP1 as well in all other prototypical phytochromes studied so far. To this end, the protonated propC has been considered a unique property of the Pfr state of bathy phytochromes.[27,28,54,55] For bathy phytochromes, it is functional for the phototransformation since the deprotonation of propC, prior to the Pr formation, initiates the secondary structure change of the sensory tongue in the PHY domain as the crucial step in the activation process of phytochromes.[28] In the bathy phytochrome Agp2, the proton acceptor is His278,[27] which is analogous to His275 in SaBphP2. Substitution of His278 with Gln or Ala shifts the pK_a of propC deprotonation in Pr from ca. 7.6 in WT to ca. 8.5 in Agp2-H278Q and Agp2-H278A, whereby the deprotonation-triggered tongue

restructuring upon Pfr → Pr transition is preserved.[27,28] A similar situation is observed in SaBphP2, where propC appears to be completely deprotonated in the WT Pr state but only partially in the H275T variant (Figure 8). It is therefore tempting to assume that the photoinduced back conversion of Pfr → Pr in SaBphP2 follows the same mechanism as in Agp2 with the secondary structure transition of the tongue initiated by the deprotonation of propC. This is in contrast to SaBphP1, which shows no protonated propC and hence no transient deprotonation in WT and the T289H variant. Evidently, in SaBphP1 as in all other prototypical phytochromes studied so far, the characteristic restructuring of the tongue during Pfr → Pr takes place via a different reaction route, regardless of His or Thr at position 289.

The unusually high pK_a of propC in the Pfr state of bathy phytochromes and its drastic lowering upon Pr formation have been attributed to specific electrostatics in the chromophore binding pocket and its changes during the photoconversion.[28,54,55] In this context, the present findings are of particular interest in view of the far-reaching similarity of the structure and amino acid composition in the chromophore binding pocket of SaBphP1 and SaBphP2 (Figure 2). In the vicinity of propC, the main difference between SaBphP1 and SaBphP2 is that the latter includes an Ala instead of Ser287. Although long-range effects cannot be ruled out completely, this substitution appears to be sufficient to perturb the local electrostatics such that the pK_a of propC increases by several units in the Pfr state of SaBphP2. The additional His275Thr substitution further increases the pK_a in Pr relative to that of the Pfr state. We thus conclude that the conserved His is an important factor in controlling the local electrostatics.

Interestingly, the Thr289His substitution in SaBphP1 also alters another pK_a, that is, that of the ring B/C N–H group in the Meta-Rc state. Here, the intensity ratio of the two RR bands between ca. 1610 and 1580 cm^{-1} that mark deprotonation of either pyrrole ring C or B is reversed upon going from SaBphP1-WT to SaBphP1-T289H (Figure 7). This finding points to a change of the ring B and C pK_a values relative to each other upon replacement of Thr289 with histidine. In contrast, the opposite substitution in SaBphP2 leaves the intensity ratio largely unchanged.

Importance of the Conserved Histidine in Other Phytochromes.

The impact of the conserved His on the structure and function can hardly be predicted a priori, as vividly illustrated by the bathy phytochromes Agp2 and *Pa*BphP (*P. aeruginosa*).[20,27,28] However, in Agp2, the effect of His278 substitution with Ala or Gln is largely restricted to the deceleration of the back reversion,[27,28] and the corresponding substitution in *Pa*BphP converts the bathy into a prototypical phytochrome with Pr being the thermodynamically stable state.[20]

In prototypical bacteriophytochomes, the effects of the His substitution are also hardly predictable. The His290Thr mutant of *Dr*BphP shows the complete tongue restructuring during the Pr → Pfr transition and thus is functionally intact despite a lower Pfr yield.[26] However, a substitution with Ala leads to a strongly reduced Pfr formation, and the photocycle is even arrested in Meta-Rc when His290 is substituted with Gln.[15]

CONCLUSIONS

His residues possess two nitrogens (Nδ, Nε) that may bind a proton. Thus, in the pH range from 6.5 to 8.0, corresponding to the physiological conditions of most eukaryotes and prokaryotes, His may exist in two neutral forms (single-protonated), a cationic form (double-protonated), and an anionic non-protonated form. Moreover, subtle alterations of the His environment may alter the actual pK_a and thus promote proton transfer. Hence, His offers a rich versatility in terms of hydrogen-bonding and electrostatic interactions which can hardly be mimicked by another single amino acid. Thus, substitution of a conserved His is expected to affect at least local properties. This is in fact also observed for the four SaBphP variants including either a His or a Thr at a critical position close to the isomerization site. The His/Thr-dependent structural differences mainly refer to hydrogen-bonding interactions with the ring D carbonyl group and, as a consequence, the torsion of the C–D methine bridge, thereby also affecting photoisomerization as already suggested previously.[26] Secondary effects appear to be related to alterations of the electrostatics in the chromophore binding pocket which in turn influence the pK_a values of ring B and C pyrrole rings and propC. None of these changes are functionally critical since they do not impair tongue restructuring as the key structural event in the photosensory domain that initiates inter-domain signal transduction in phytochromes. Moreover, the presence of the conserved His does not categorically decide on reaction mechanisms. Both SaBphP2 variants (with His or Thr at position 275) appear to follow the well-characterized Pfr → Pr photoconversion route of bathy phytochromes in which deprotonation of propC triggers the secondary structure transition of the tongue, whereas SaBphP1 (WT and the T289H variant) favors the photoconversion route of prototypical phytochromes. Altogether, we therefore conclude that His may play an important but not indispensable role for the function of phytochromes, which in addition appears to be highly context-dependent. Specifically, in SaBphP1 and SaBphP2, the His/Thr exchange may serve for fine tuning of spectral and mechanistic properties. Also, the effects of the His/Thr substitutions are rather mild, possibly because both residues are polar and capable of undergoing hydrogen-bonding interactions. This is in contrast to the more drastic effects of His substitution by residues with quite different polarity and hydrophobicity such as Ala.[15]

Supplementary Material

Refer to Web version on PubMed Central for supplementary material.

ACKNOWLEDGMENTS

This work was supported by the Deutsche Forschungsgemeinschaft (DFG) through the CRC 1078 “Protonation Dynamics in Protein Function” (project B06 to P.H. and P.S.) and by NSF-MCB-RUI 1413360, NSF-MCB-EAGER grant 1839513, and NSF STC BioXFEL center award 6227 (to E.A.S.). M.N. training was supported in part by the National Institute of General Medical Sciences (NIGMS) of the National Institutes of Health (NIH) Maximizing Access to Research Careers (MARC) T34 GM105549 grant to E.A.S. Further support was obtained from the Einstein Center of Catalysis EC^2 (to P.H. and P.S.).

REFERENCES

(1). Briggs WR; Rice HV Phytochrome: Chemical and Physical Properties and Mechanism of Action. Annu. Rev. Plant Physiol 1972, 23, 293–334.

(2). Rockwell NC; Su Y-S; Lagarias JC Phytochrome Structure and Signaling Mechanisms. Annu. Rev. Plant Biol 2006, 57, 837–858. [PubMed: 16669784]

(3). Wang H; Wang H Phytochrome Signaling: Time to Tighten up the Loose Ends. Mol. Plant 2015, 8, 540–551. [PubMed: 25670340]

(4). Lamparter T; Krauß N; Scheerer P Phytochromes from Agrobacterium Fabrum. Photochem. Photobiol 2017, 93, 642–655. [PubMed: 28500698]

(5). Hughes J Phytochrome Three-Dimensional Structures and Functions. Biochem. Soc. Trans 2010, 38, 710–716. [PubMed: 20298248]

(6). Sineshchekov VA Photobiophysics and Photobiochemistry of the Heterogeneous Phytochrome System. Biochim. Biophys. Acta 1995, 1228, 125–164.

(7). Rockwell NC; Lagarias JC The Structure of Phytochrome: A Picture Is Worth a Thousand Spectra. Plant Cell 2006, 18, 4–14. [PubMed: 16387836]

(8). Andel F; Lagarias JC; Mathies RA Resonance Raman Analysis of Chromophore Structure in the Lumi-R Photoproduct of Phytochrome. Biochemistry 1996, 35, 15997–16008. [PubMed: 8973170]

(9). Kneip C; Hildebrandt P; Schlamann W; Braslavsky SE; Mark F; Schaffner K Protonation State and Structural Changes of the Tetrapyrrole Chromophore during the Pr → Pfr Phototransformation of Phytochrome: A Resonance Raman Spectroscopic Study. Biochemistry 1999, 38, 15185–15192. [PubMed: 10563801]

(10). Mizutani Y; Tokutomi S; Kitagawa T Resonance Raman Spectra of the Intermediates in Phototransformation of Large Phytochrome: Deprotonation of the Chromophore in the Bleached Intermediate. Biochemistry 1994, 33, 153–158. [PubMed: 8286333]

(11). Borucki B; von Stetten D; Seibeck S; Lamparter T; Michael N; Mroginski MA; Otto H; Murgida DH; Heyn MP; Hildebrandt P Light-Induced Proton Release of Phytochrome Is Coupled to the Transient Deprotonation of the Tetrapyrrole Chromophore. J. Biol. Chem 2005, 280, 34358–34364. [PubMed: 16061486]

(12). Takala H; Björling A; Berntsson O; Lehtivuori H; Niebling S; Hoernke M; Kosheleva I; Henning R; Menzel A; Ihalainen JA; Westenhoff S Signal Amplification and Transduction in Phytochrome Photosensors. Nature 2014, 509, 245–248. [PubMed: 24776794]

(13). Gourinchas G; Etzl S; Göbl C; Vide U; Madl T; Winkler A Long-Range Allosteric Signaling in Red Light–Regulated Diguanylyl Cyclases. Sci. Adv 2017, 3, No. e1602498. [PubMed: 28275738]

(14). Gourinchas G; Heintz U; Winkler A Asymmetric Activation Mechanism of a Homodimeric Red Light-Regulated Photoreceptor. eLife 2018, 7, No. e34815. [PubMed: 29869984]

(15). Wagner JR; Zhang J; von Stetten D; Günther M; Murgida DH; Mroginski MA; Walker JM; Forest KT; Hildebrandt P; Vierstra RD Mutational Analysis of Deinococcus Radiodurans Bacteriophytochrome Reveals Key Amino Acids Necessary for the Photochromicity and Proton Exchange Cycle of Phytochromes. J. Biol. Chem 2008, 283, 12212–12226. [PubMed: 18192276]

(16). Von Stetten D; Seibeck S; Michael N; Scheerer P; Mroginski MA; Murgida DH; Krauss N; Heyn MP; Hildebrandt P; Borucki B; Lamparter T Highly Conserved Residues Asp-197 and His-250 in Agp1 Phytochrome Control the Proton Affinity of the Chromophore and Pfr Formation. J. Biol. Chem 2007, 282, 2116–2123. [PubMed: 17121858]

(17). Schmidt A; Sauthof L; Szczepek M; Lopez MF; Escobar FV; Qureshi BM; Michael N; Buhrke D; Stevens T; Kwiatkowski D; von Stetten D; Mroginski MA; Krauß N; Lamparter T; Hildebrandt P; Scheerer P Structural Snapshot of a Bacterial Phytochrome in Its Functional Intermediate State. Nat. Commun 2018, 9, 4912. [PubMed: 30464203]

(18). Yang X; Kuk J; Moffat K Crystal Structure of Pseudomonas Aeruginosa Bacteriophytochrome: Photoconversion and Signal Transduction. Proc. Natl. Acad. Sci. U.S.A 2008, 105, 14715–14720. [PubMed: 18799746]

(19). Burgie ES; Bussell AN; Walker JM; Dubiel K; Vierstra RD Crystal Structure of the Photosensing Module from a Red/Far-Red Light-Absorbing Plant Phytochrome. Proc. Natl. Acad. Sci. U.S.A 2014, 111, 10179–10184. [PubMed: 24982198]

(20). Yang X; Kuk J; Moffat K Conformational Differences between the Pfr and Pr States in Pseudomonas Aeruginosa Bacteriophytochrome. Proc. Natl. Acad. Sci. U.S.A 2009, 106, 15639–15644. [PubMed: 19720999]

(21). Wagner JR; Brunzelle JS; Forest KT; Vierstra RD A Light-Sensing Knot Revealed by the Structure of the Chromophore-Binding Domain of Phytochrome. Nature 2005, 438, 325–331. [PubMed: 16292304]

(22). Yang X; Stojkovic EA; Kuk J; Moffat K Crystal Structure of the Chromophore Binding Domain of an Unusual Bacteriophytochrome, RpBphP3, Reveals Residues That Modulate Photoconversion. Proc. Natl. Acad. Sci. U.S.A 2007, 104, 12571–12576. [PubMed: 17640891]

(23). Essen L-O; Mailliet J; Hughes J The Structure of a Complete Phytochrome Sensory Module in the Pr Ground State. Proc. Natl. Acad. Sci. U.S.A 2008, 105, 14709–14714. [PubMed: 18799745]

(24). Burgie ES; Zhang J; Vierstra RD Crystal Structure of Deinococcus Phytochrome in the Photoactivated State Reveals a Cascade of Structural Rearrangements during Photoconversion. Structure 2016, 24, 448–457. [PubMed: 26853942]

(25). Nagano S; Scheerer P; Zubow K; Michael N; Inomata K; Lamparter T; Krauß N The Crystal Structures of the N-Terminal Photosensory Core Module of Agrobacterium Phytochrome Agp1 as Parallel and Anti-Parallel Dimers. J. Biol. Chem 2016, 291, 20674–20691. [PubMed: 27466363]

(26). Lenngren N; Edlund P; Takala H; Stucki-Buchli B; Rumfeldt J; Peshev I; Häkkänen H; Westenhoff S; Ihalainen JA Coordination of the Biliverdin D-Ring in Bacteriophytochromes. Phys. Chem. Chem. Phys 2018, 20, 18216–18225. [PubMed: 29938729]

(27). Velazquez Escobar F; Piwowarski P; Salewski J; Michael N; Fernandez Lopez M; Rupp A; Qureshi BM; Scheerer P; Bartl F; Frankenberg-Dinkel N; Siebert F; Andrea Mroginski M; Hildebrandt P A Protonation-Coupled Feedback Mechanism Controls the Signalling Process in Bathy Phytochromes. Nat. Chem 2015, 7, 423–430. [PubMed: 25901821]

(28). Kraskov A; Nguyen AD; Goerling J; Buhrke D; Velazquez Escobar F; Fernandez Lopez M; Michael N; Sauthof L; Schmidt A; Piwowarski P; Yang Y; Stensitzki T; Adam S; Bartl F; Schapiro I; Heyne K; Siebert F; Scheerer P; Mroginski MA; Hildebrandt P Intramolecular Proton Transfer Controls Protein Structural Changes in Phytochrome. Biochemistry 2020, 59, 1023–1037. [PubMed: 32073262]

(29). Woitowich NC; Halavaty AS; Waltz P; Kupitz C; Valera J; Tracy G; Gallagher KD; Claesson E; Nakane T; Pandey S; Nelson G; Tanaka R; Nango E; Mizohata E; Owada S; Tono K; Joti Y; Nugent AC; Patel H; Mapara A; Hopkins J; Duong P; Bizhga D; Kovaleva SE; St. Peter R; Hernandez CN; Ozarowski WB; Roy-Chowdhuri S; Yang J-H; Edlund P; Takala H; Ihalainen J; Brayshaw J; Norwood T; Poudyal I; Fromme P; Spence JCH; Moffat K; Westenhoff S; Schmidt M; Stojković EA Structural Basis for Light Control of Cell Development Revealed by Crystal Structures of a Myxobacterial Phytochrome. IUCrJ 2018, 5, 619–634.

(30). Sanchez JC; Carrillo M; Pandey S; Noda M; Aldama L; Feliz D; Claesson E; Wahlgren WY; Tracy G; Duong P; Nugent AC; Field A;Šrajer V; Kupitz C; Iwata S; Nango E; Tanaka R; Tanaka T; Fangjia L; Tono K; Owada S; Westenhoff S; Schmidt M; Stojković EA High-Resolution Crystal Structures of a Myxobacterial Phytochrome at Cryo and Room Temperatures. Struct. Dyn 2019, 6, 054701. [PubMed: 31559319]

(31). Björling A; Berntsson O; Takala H; Gallagher KD; Patel H; Gustavsson E; St. Peter R; Duong P; Nugent A; Zhang F; Berntsen P; Appio R; Rajkovic I; Lehtivuori H; Panman MR; Hoernke M; Niebling S; Harimoorthy R; Lamparter T; Stojković EA; Ihalainen JA; Westenhoff S Ubiquitous Structural Signaling in Bacterial Phytochromes. J. Phys. Chem. Lett 2015, 6, 3379–3383. [PubMed: 26275765]

(32). Carrillo M; Pandey S; Sanchez J; Noda M; Poudyal I; Aldama L; Malla TN; Claesson E; Wahlgren WY; Feliz D; Šrajer V; Maj M; Castillon L; Iwata S; Nango E; Tanaka R; Tanaka T; Fangjia L; Tono K; Owada S; Westenhoff S; Stojković EA; Schmidt M High-Resolution Crystal Structures of Transient Intermediates in the Phytochrome Photocycle. Structure 2021, 29, 743. [PubMed: 33756101]

(33). Lamparter T; Michael N; Mittmann F; Esteban B Phytochrome from Agrobacterium Tumefaciens Has Unusual Spectral Properties and Reveals an N-Terminal Chromophore Attachment Site. Proc. Natl. Acad. Sci. U.S.A 2002, 99, 11628–11633. [PubMed: 12186972]

(34). Schumann C; Groß R; Michael N; Lamparter T; Diller R Sub-Picosecond Mid-Infrared Spectroscopy of Phytochrome Agp1 from Agrobacterium Tumefaciens. ChemPhysChem 2007, 8, 1657–1663. [PubMed: 17614346]

(35). von Stetten D; Günther M; Scheerer P; Murgida DH; Mroginski MA; Krauß N; Lamparter T; Zhang J; Anstrom DM; Vierstra RD; Forest KT; Hildebrandt P Chromophore Heterogeneity and Photoconversion in Phytochrome Crystals and Solution Studied by Resonance Raman Spectroscopy. Angew. Chem., Int. Ed 2008, 47, 4753–4755.

(36). Borucki B; Lamparter T A Polarity Probe for Monitoring Light-Induced Structural Changes at the Entrance of the Chromophore Pocket in a Bacterial Phytochrome. J. Biol. Chem 2009, 284, 26005–26016. [PubMed: 19640848]

(37). Piwowarski P; Ritter E; Hofmann K-P; Hildebrandt P; von Stetten D; Scheerer P; Michael N; Lamparter T; Bartl F Light-Induced Activation of Bacterial Phytochrome Agp1 Monitored by Static and Time-Resolved FTIR Spectroscopy. ChemPhysChem 2010, 11, 1207–1214. [PubMed: 20333618]

(38). Takiden A; Velazquez-Escobar F; Dragelj J; Woelke AL; Knapp E-W; Piwowarski P; Bart F; Hildebrandt P; Mroginski MA Structural and Vibrational Characterization of the Chromophore Binding Site of Bacterial Phytochrome Agp1. Photochem. Photobiol 2017, 93, 713–723. [PubMed: 28500721]

(39). Scheerer P; Michael N; Park JH; Noack S; Förster C; Hammam MAS; Inomata K; Choe H-W; Lamparter T; Krauß N Crystallization and Preliminary X-Ray Crystallographic Analysis of the N-Terminal Photosensory Module of Phytochrome Agp1, a Biliverdin-Binding Photoreceptor from Agrobacterium Tumefaciens. J. Struct. Biol 2006, 153, 97–102. [PubMed: 16377207]

(40). Velazquez Escobar F; Kneip C; Michael N; Hildebrandt T; Tavraz N; Gärtner W; Hughes J; Friedrich T; Scheerer P; Mroginski MA; Hildebrandt P The Lumi-R Intermediates of Prototypical Phytochromes. J. Phys. Chem. B 2020, 124, 4044–4055. [PubMed: 32330037]

(41). Hall TA BioEdit: A User-Friendly Biological Sequence Alinment Editor and Analysis Program for Windows 95/98/NT. Nucleic Acids Symp. Ser 1999, 41, 95–98.

(42). Salewski J; Escobar FV; Kaminski S; Von Stetten D; Keidel A; Rippers Y; Michael N; Scheerer P; Piwowarski P; Bartl F; Frankenberg-Dinkel N; Ringsdorf S; Gärtner W; Lamparter T; Mroginski MA; Hildebrandt P Structure of the Biliverdin Cofactor in the Pfr State of Bathy and Prototypical Phytochromes. J. Biol. Chem 2013, 288, 16800–16814. [PubMed: 23603902]

(43). Mroginski MA; Kaminski S; Von Stetten D; Ringsdorf S; Gärtner W; Essen L-O; Hildebrandt P Structure of the Chromophore Binding Pocket in the Pr State of Plant Phytochrome PhyA. J. Phys. Chem. B 2011, 115, 1220–1231. [PubMed: 21192668]

(44). Velazquez Escobar F; Hildebrandt T; Utesch T; Schmitt FJ; Seuffert I; Michael N; Schulz C; Mroginski MA; Friedrich T; Hildebrandt P Structural Parameters Controlling the Fluorescence Properties of Phytochromes. Biochemistry 2013, 53, 20–29. [PubMed: 24328165]

(45). Mathes T; Ravensbergen J; Kloz M; Gleichmann T; Gallagher KD; Woitowich NC; St. Peter R; Kovaleva SE; Stojković EA; Kennis JTM Femto- to Microsecond Photodynamics of an Unusual Bacteriophytochrome. J. Phys. Chem. Lett 2015, 6, 239–243. [PubMed: 26263456]

(46). Smit K; Matysik J; Hildebrandt P; Mark F Vibrational Analysis of Biliverdin Dimethyl Ester. J. Phys. Chem 1993, 97, 11887–11900.

(47). Matysik J; Hildebrandt P; Smit K; Mark F; Gärtner W; Braslavsky SE; Schaffner K; Schrader B Raman Spectroscopic Analysis of Isomers of Biliverdin Dimethyl Ester. J. Pharm. Biomed. Anal 1997, 15, 1319–1324. [PubMed: 9226559]

(48). Kneip C; Hildebrandt P; Németh K; Mark F; Schaffner K Interpretation of the Resonance Raman Spectra of Linear Tetrapyrroles Based on DFT Calculations. Chem. Phys. Lett 1999, 311, 479–484.

(49). Stojković EA; Toh KC; Alexandre MT; Baclayon M; Moffat K; Kennis JT FTIR Spectroscopy Revealing Light-Dependent Refolding of the Conserved Tongue Region of Bacteriophytochrome. J. Phys. Chem. Lett 2014, 5, 2512–2515. [PubMed: 25126387]

(50). Schwinté P; Gärtner W; Sharda S; Mroginski M-A; Hildebrandt P; Siebert F; Hildebrandt P; Sharda S; Gärtner W The Photoreactions of Recombinant Phytochrome CphA from the Cyanobacterium Calothrix PCC7601: A Low-Temperature UV-Vis and FTIR Study. Photochem. Photobiol 2009, 85, 239–249. [PubMed: 18764898]

(51). Schwinté P; Foerstendorf H; Hussain Z; Gärtner W; Mroginski M-A; Hildebrandt P; Siebert F FTIR Study of the Photoinduced Processes of Plant Phytochrome Phya Using Isotope-Labeled Bilins and Density Functional Theory Calculations. Biophys. J 2008, 95, 1256–1267. [PubMed: 18390618]

(52). Siebert F; Grimm R; Rüdiger W; Schmidt G; Scheer H Infrared Spectroscopy of Phytochrome and Model Pigments. Eur. J. Biochem 1990, 194, 921–928. [PubMed: 2269310]

(53). Van Thor JJ; Fisher N; Rich PR Assignments of the Pfr - Pr FTIR Difference Spectrum of Cyanobacterial Phytochrome Cph1 Using15N And 13C Isotopically Labeled Phycocyanobilin Chromophore. J. Phys. Chem. B 2005, 109, 20597–20604. [PubMed: 16853666]

(54). Velázquez Escobar F; Buhrke D; Michael N; Sauthof L; Wilkening S; Tavraz NN; Salewski J; Frankenberg-Dinkel N; Mroginski MA; Scheerer P; Friedrich T; Siebert F; Hildebrandt P Common Structural Elements in the Chromophore Binding Pocket of the Pfr State of Bathy Phytochromes. Photochem. Photobiol 2017, 93, 724–732. [PubMed: 28500706]

(55). Fernandez Lopez M; Nguyen AD; Velazquez Escobar F; González R; Michael N; Nogacz Ż; Piwowarski P; Bartl F; Siebert F; Heise I; Scheerer P; Gärtner W; Mroginski MA; Hildebrandt P Role of the Propionic Side Chains for the Photoconversion of Bacterial Phytochromes. Biochemistry 2019, 58, 3504–3519. [PubMed: 31348653]

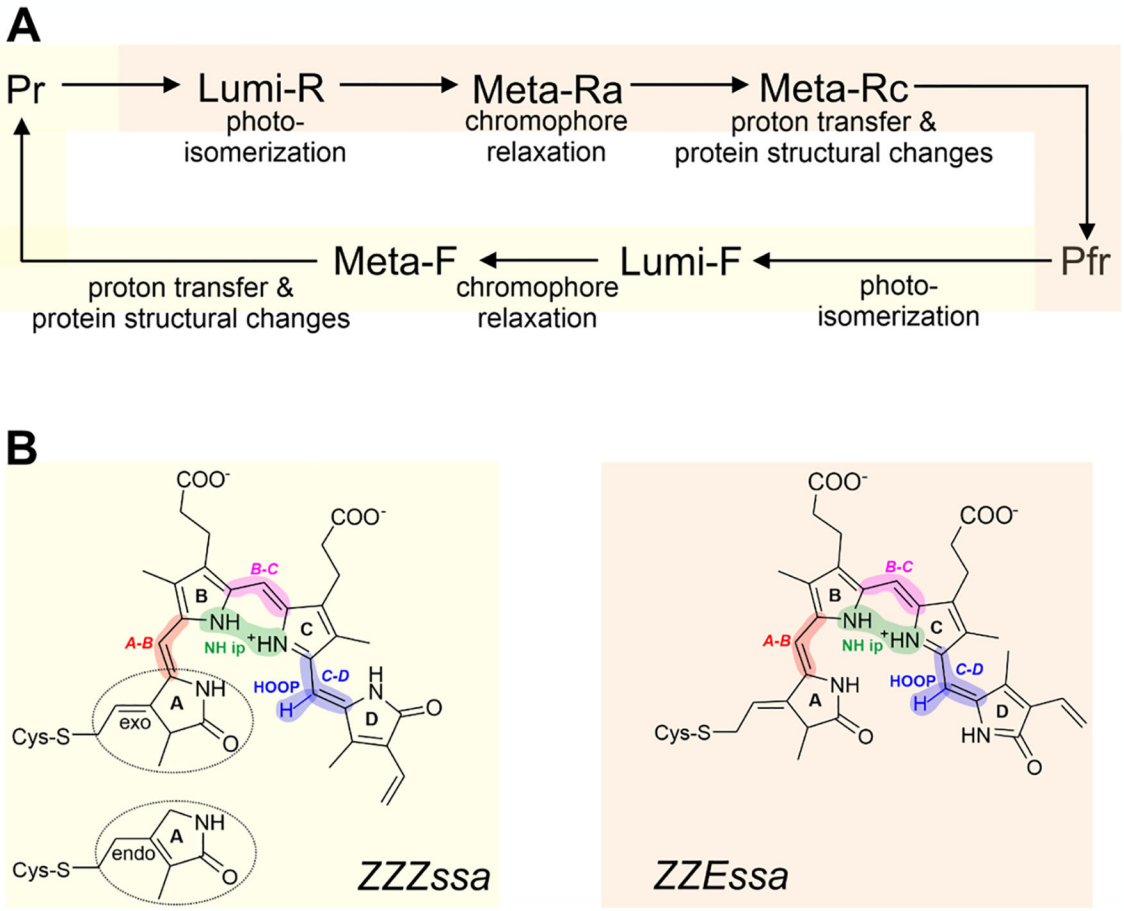

Figure 1.

(A) Reaction sequence of the Pr → Pfr phototransformation and its photoinduced back reaction. The yellow- and red-shaded species refer to states with *ZZZssa* and *ZZEssa* chromophore configurations, respectively. Both configurations are shown in (B), also indicating the exocyclic double bond of ring A after covalent binding to a Cys side chain of the protein. For the *ZZZssa* configuration (B, left), also, the endocyclic double-bond attachment mode is shown as it is found for Agp1. The blue, magenta, and red colors highlight the C–D, B–C, and A–B methine bridges, respectively. These same colors were used in Figures 3–8 in the RR and IR spectra to indicate the respective localization of the modes. Correspondingly, the green color (N–H groups of rings B and C) is used to mark the corresponding NH ip mode.

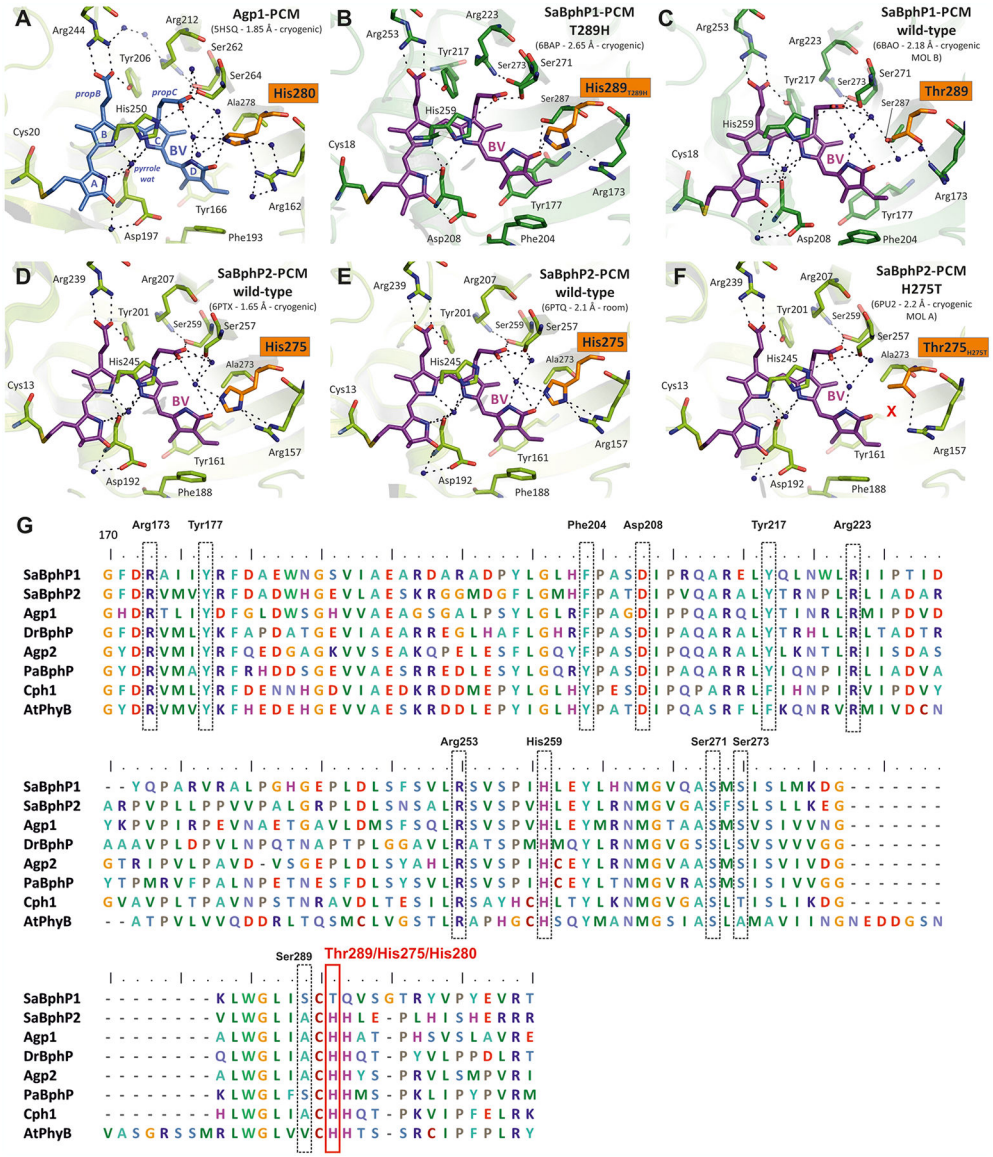

Figure 2.

Chromophore binding pocket with several essential BV binding partners. (A–F) All structures represent the Pr states. The BV chromophores are depicted as sticks, relevant water molecules are shown as blue spheres, and all proteins are shown in ribbons including essential binding amino acids, which are also represented as sticks. The relevant His or Thr at ring D of BV is depicted as orange sticks. (A) Agp1-PCM of *A. fabrum* [PDB entry 5HSQ with 1.85 Å resolution at CT, color code: BV (blue); protein (chartreuse green)]. (B–F) *S. aurantiaca* phytochromes (B) SaBphP1-PCM-T289H [PDB entry 6BAP with 2.65 Å resolution, CT, color code: BV (purple); protein (dark green)]. (C) WT SaBphP1-PCM [PDB entry 6BAO with 2.18 Å resolution, molecule B, CT, color code: BV (purple); protein (dark green)]. (D) WT SaBphP2-PCM [PDB entry 6PTX with 1.65 Å resolution, CT, color code: BV (purple); protein (dark green)]. (E) WTSaBphP2-PCM [PDB entry 6PTQ with 2.1 Å resolution, recorded at room temperature, color code: BV

(purple); protein (dark green)]. (F) SaBphP2-PCM-H275T [PDB entry 6PU2 with 2.2 Å resolution, molecule A, CT, color code: BV (purple); protein (dark green)]. (G) Partial sequence alignment of selected phytochromes: prototypical bacteriophytochromes (SaBphP1 and SaBphP2 from *S. aurantiaca*, Agp1 from *A. fabrum*, DrBphP from *D. radiodurans*), bathy bacteriophytochromes (Agp2 from *A. fabrum*, PaBphP from *P. aeruginosa*), the cyanobacterial phytochrome (Cph1 from *Synechocystis* sp. *PCC 6803*), and the plant phytochrome (AtPhyB from *Arabidopsis thaliana*). Important conserved amino acids of the chromophore pocket, as visualized in A–F, are highlighted in black boxes (except for Cys18). The numbering is related to the WT SaBphP1 (starting at position 170). The relevant position Thr289 for SaBphP1 is shown in a red box (His275 in SaBphP2 and His280 in Agp1). The red X in F indicates that there is no direct hydrogen-bond interaction from ring D of BV to Thr in the case of a Thr-containing SaBphP2 structure.

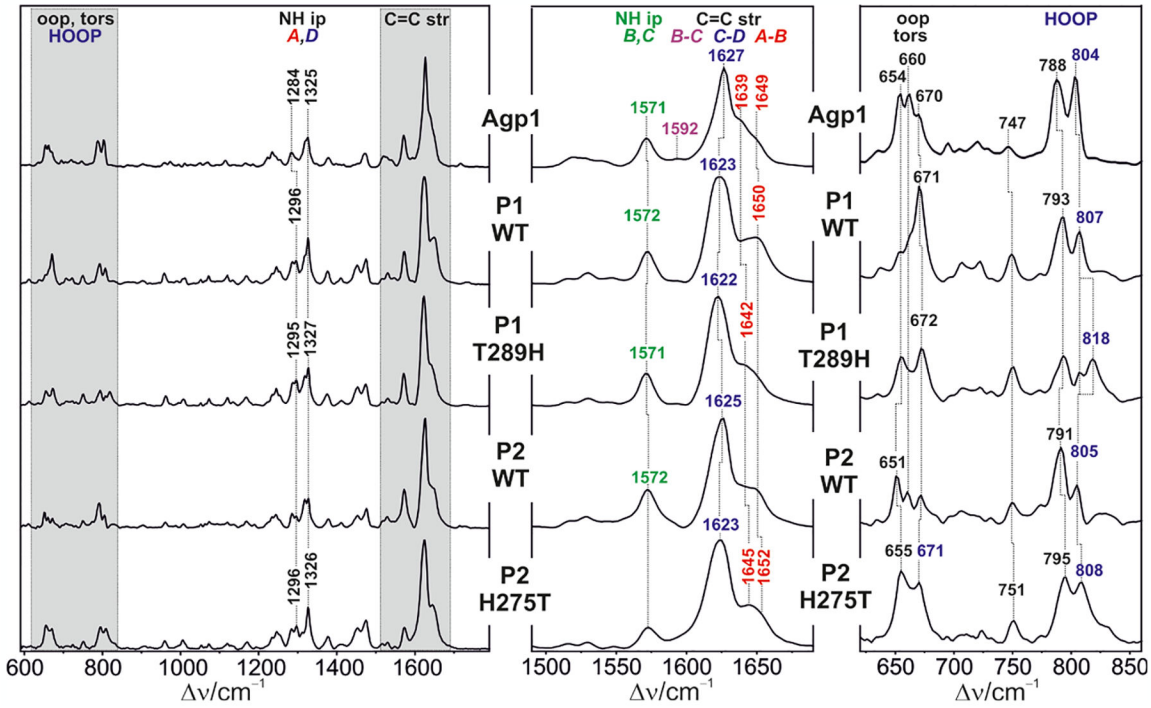

Figure 3.

RR spectra of the Pr state of the PCM constructs from the following phytochromes: Agp1-WT (Agp1), SaBphP1-WT (P1-WT), SaBphP1-T289H (P1-T289H), SaBphP2-WT (P2-WT), and SaBphP2-H275T (P2-H275T) in H_2O. The C=C stretching and HOOP regions are shown on an expanded scale in the middle and right panels, respectively. The color code of the frequency labels is explained in Figure 1. Spectra were recorded at 140 K.

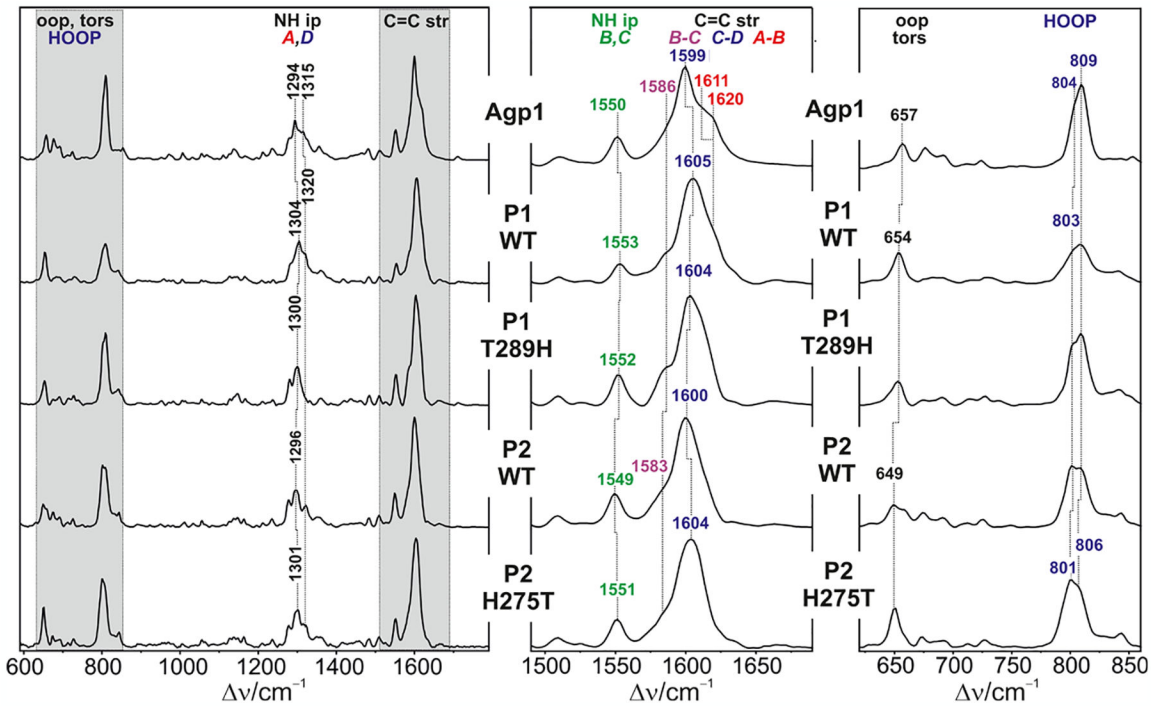

Figure 4.

RR spectra of the Pfr state of the PCM constructs from the following phytochromes: Agp1-WT (Agp1), SaBphP1-WT (P1-WT), SaBphP1-T289H (P1-T289H), SaBphP2-WT (P2-WT), and SaBphP2-H275T (P2-H275T) in H_2O. The C=C stretching and HOOP regions are shown on an expanded scale in the middle and right panels, respectively. The color code of the frequency labels is explained in Figure 1. Spectra were recorded at 140 K.

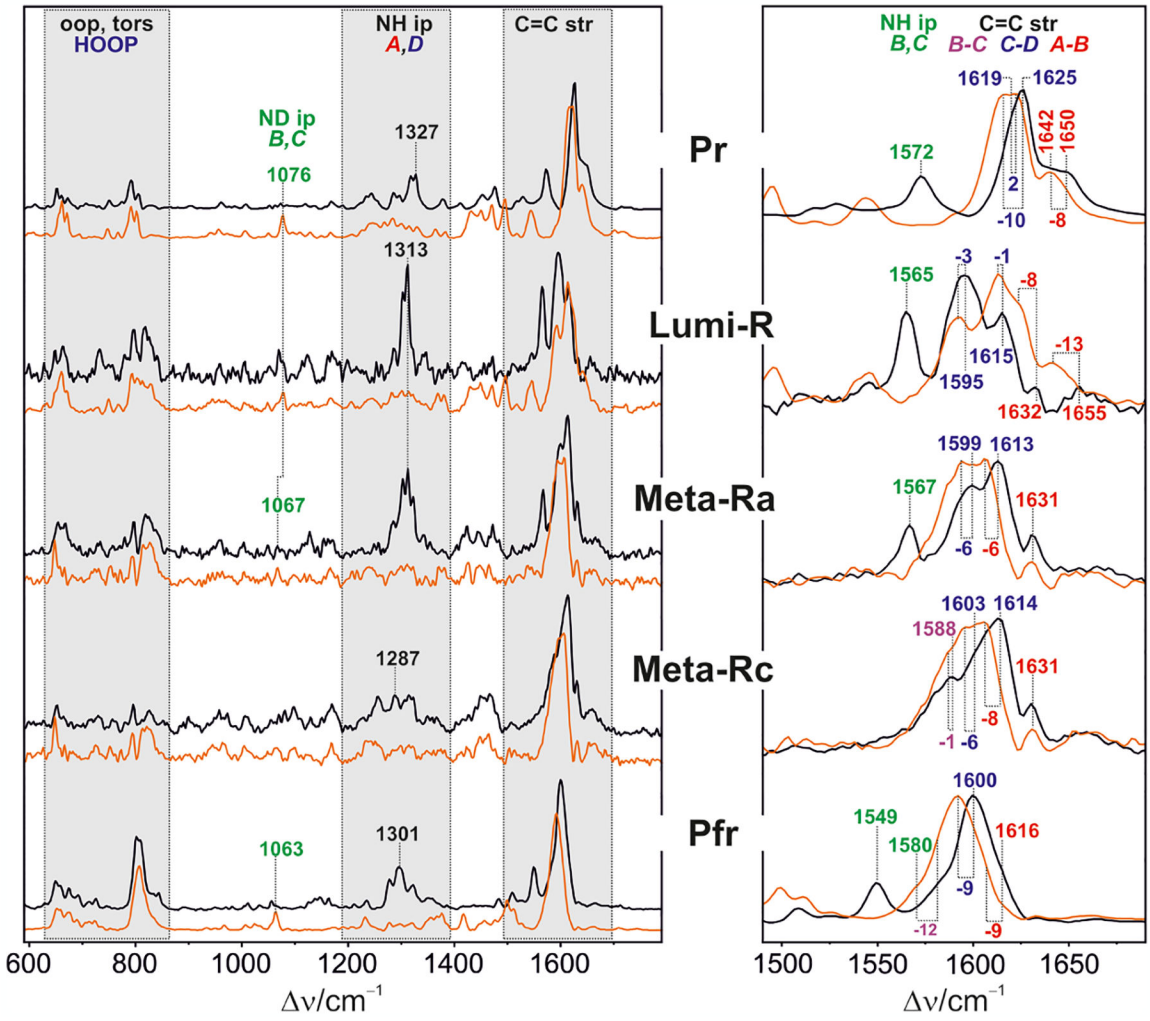

Figure 5.

RR spectra of SaBphP2-PCM-WT in the various states of the Pr → Pfr photoconversion, all measured at 140 K from samples in H_2O (black) and D_2O (orange). The C=C stretching region is shown on an expanded scale in the right panel. The frequency labels refer to bands in H_2O and their shifts upon H/D exchange using the color code as explained in Figure 1.

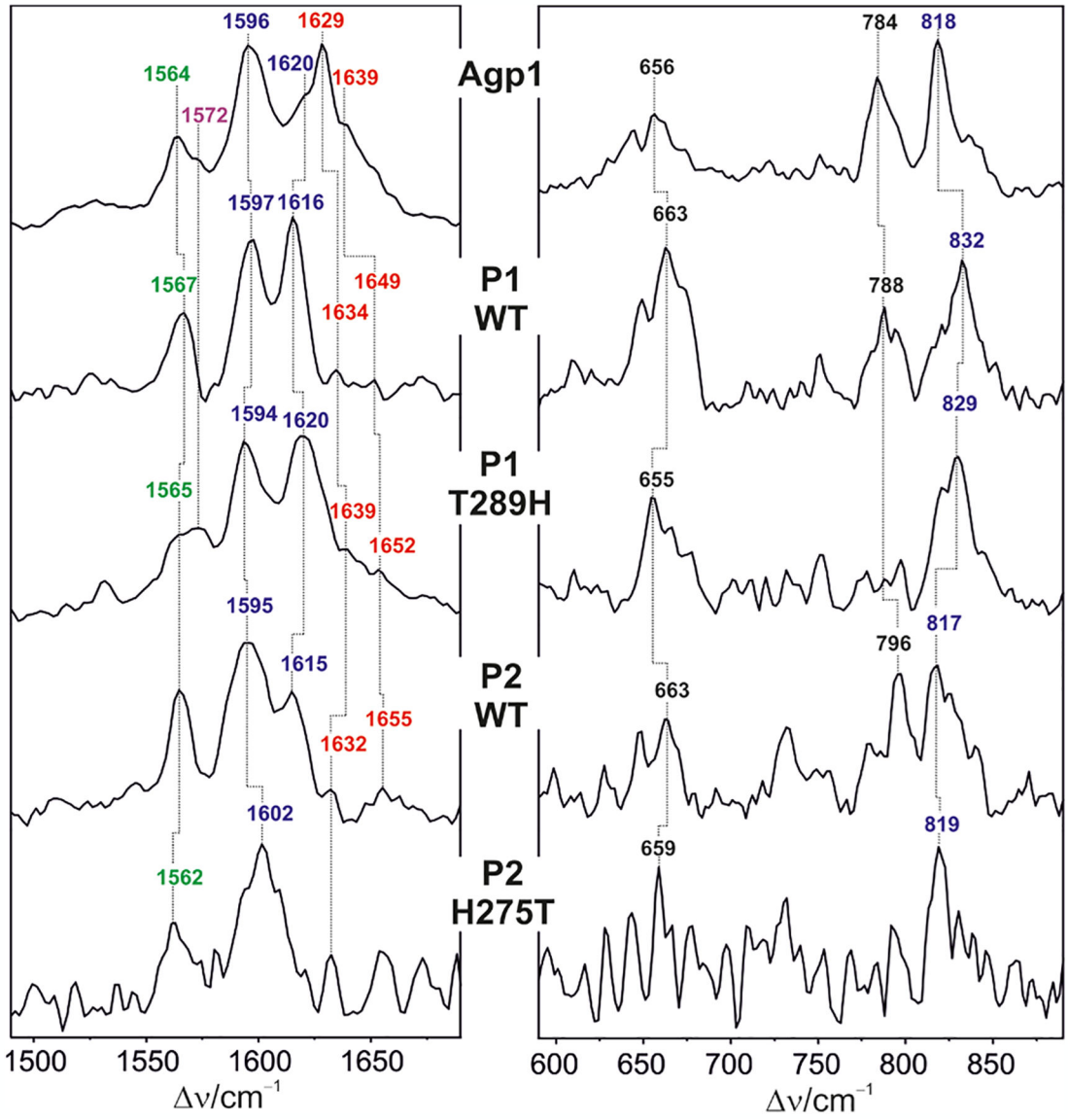

Figure 6.

RR spectra of the Lumi-R state of the PCM constructs from the following phytochromes: Agp1-WT (Agp1), SaBphP1-WT (P1-WT), SaBphP1-T289H (P1-T289H), SaBphP2-WT (P2-WT), and SaBphP2-H275T (P2-H275T) in H_2O, showing the C=C stretching (left) and HOOP (right) regions. The color code of the frequency labels is explained in Figure 1. Spectra were recorded at 140 K.

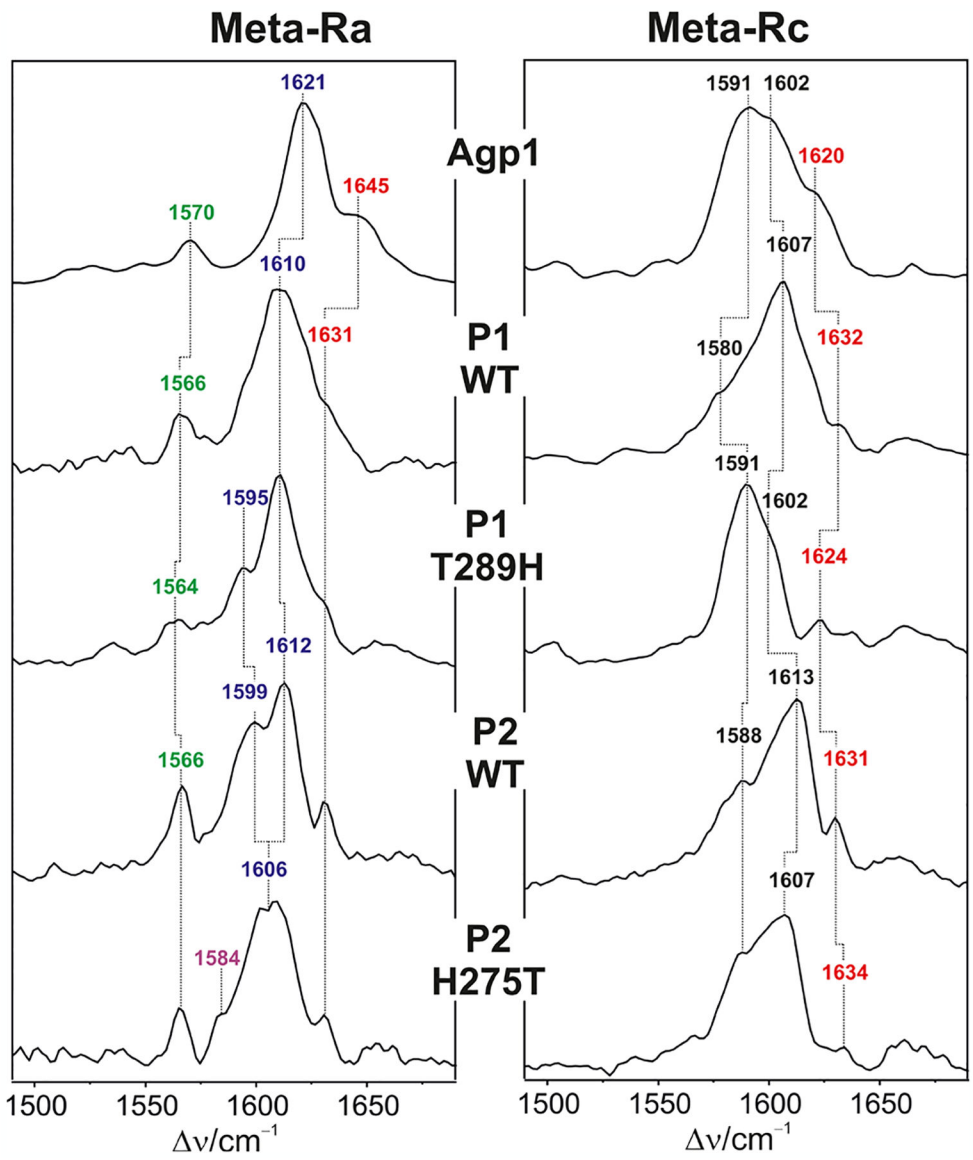

Figure 7.

RR spectra of the Meta-Ra (left) and Meta-Rc (right) states of Agp1-PCM-WT (Agp1), SaBphP1-PCM-WT (P1-WT), SaBphP1-PCM-T289H (P1-T289H), SaBphP2-PCM-WT (P2-WT), and SaBphP2-PCM-H275T (P2-H275T) in H_2O, showing the C=C stretching region. The color code of the frequency labels is explained in Figure 1. Spectra were recorded at 140 K.

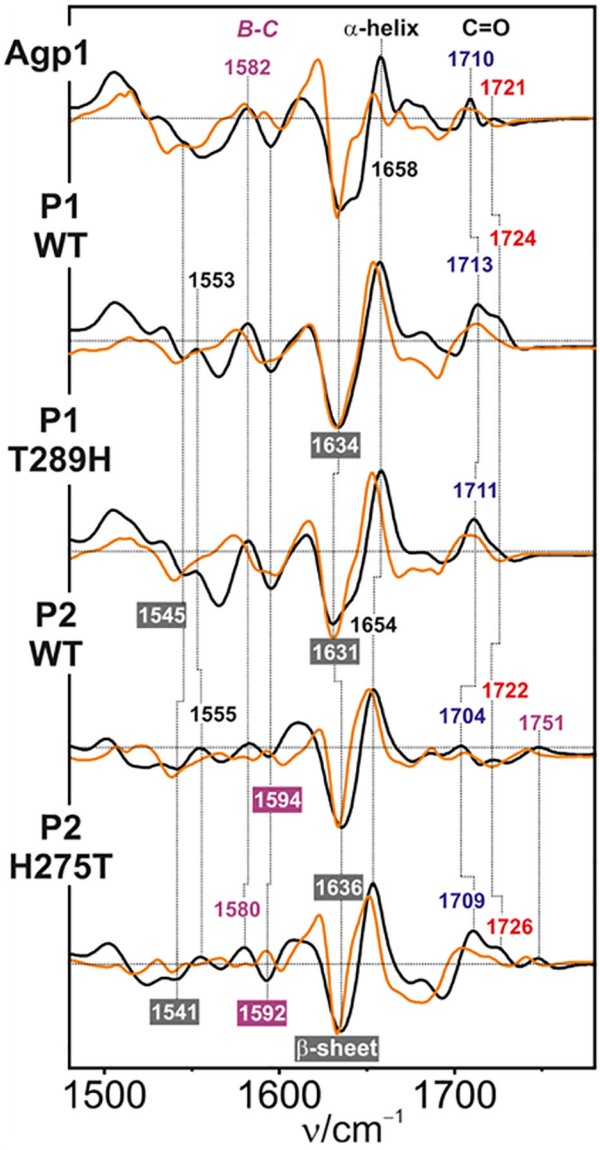

Figure 8.

IR difference spectra of the Pr (negative signals, labels in gray-shaded boxes) to Pfr (positive signals) of Agp1-PCM-WT (Agp1), SaBphP1-PCM-WT (P1-WT), SaBphP1-PCM-T289H (P1-T289H), SaBphP2-PCM-WT (P2-WT), and SaBphP2-PCM-H275T (P2-H275T) in H_2O (black) and D_2O (orange), obtained at 293 K. The color code is adapted from Figure 1, with the red- and blue-labeled bands referring to the C=O stretching of rings A and D, respectively.

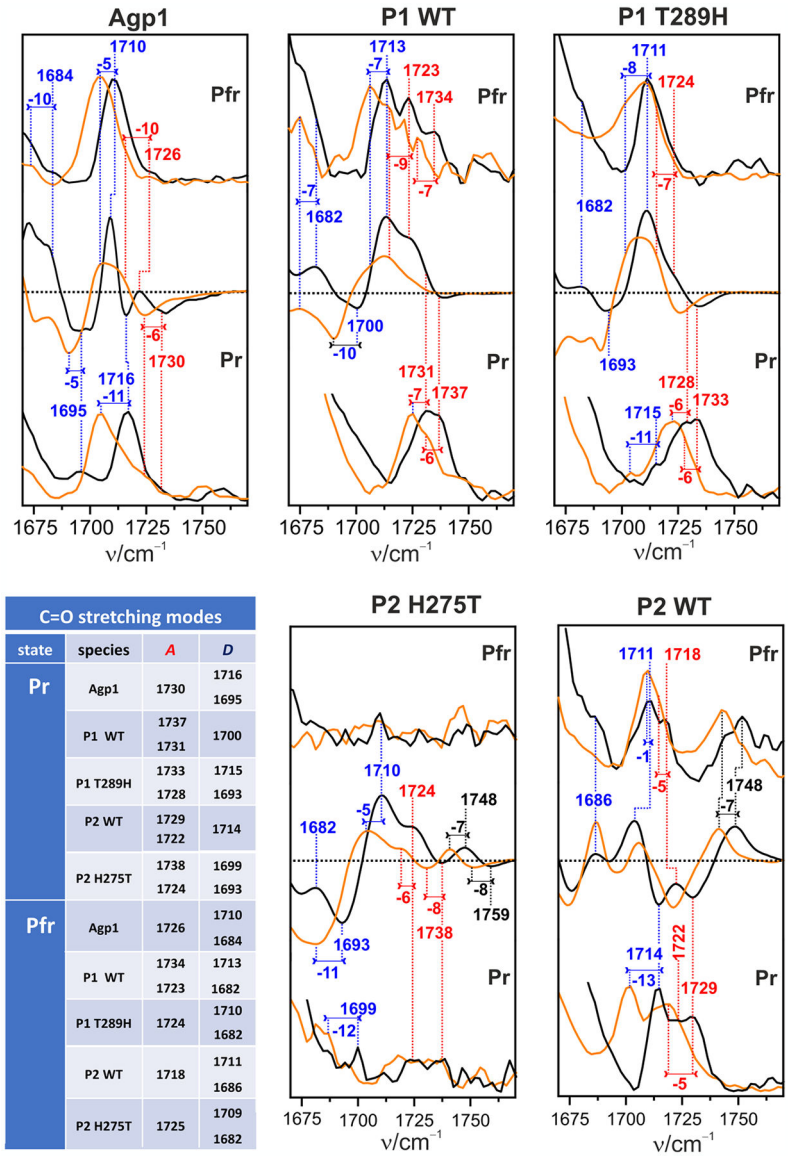

C=O stretching modes			
state	species	A	D
Pr	Agp1	1730	1716 1695
	P1 WT	1737 1731	1700
	P1 T289H	1733 1728	1715 1693
	P2 WT	1729 1722	1714
	P2 H275T	1738 1724	1699 1693
Pfr	Agp1	1726	1710 1684
	P1 WT	1734 1723	1713 1682
	P1 T289H	1724	1710 1682
	P2 WT	1718	1711 1686
	P2 H275T	1725	1709 1682

Figure 9.

RR spectra, recorded at 140 K, and IR "Pfr minus Pr" difference spectra, recorded at 293 K, of Agp1-PCM-WT (Agp1), SaBphP1-PCM-WT (P1-WT), SaBphP1-PCM-T289H (P1-T289H), SaBphP2-PCM-WT (P2-WT), and SaBphP2-PCM-H275T (P2-H275T) in H_2O (black) and D_2O (orange). The spectra show the C=O stretching region with red and blue labels, indicating the corresponding modes of rings A and D, respectively. The black label indicates the C=O stretching of the protonated prop*C*. In each panel, the RR spectra of the Pfr and Pr states are given by the top and bottom traces, respectively. The middle trace refers to the IR difference spectra with positive and negative signals corresponding to Pfr and Pr, respectively. The spectra were scaled to improve the clarity of the presentation. The bottom left panel summarizes the frequencies of the ring A and D C=O stretching modes (in cm^{-1}).